Optical constraints on two-photon voltage imaging

Hunter C. Davis*, F. Phil Brooks III*, J. David Wong-Campos, Adam E. Cohen

Department of Chemistry and Chemical Biology, Harvard University

Correspondence: cohen@chemistry.harvard.edu

Abstract

Genetically encoded voltage indicators (GEVIs) are a valuable tool for studying neural circuits *in vivo*, but the relative merits of one-photon (1P) vs. two-photon (2P) voltage imaging are not well characterized. Here we compare the photophysical and imaging properties of commonly used GEVIs under 1P and 2P excitation. 2P excitation requires ~10^4-fold more illumination power per cell to produce comparable photon count rates to 1P excitation, driving a stringent tradeoff between shot noise and tissue photodamage.

Main

A longstanding dream in neuroscience has been to record the membrane potential of hundreds or thousands of neurons simultaneously in a behaving animal. Such measurements could reveal functional connections, probe input-output properties of cells and of microcircuits, and help discern principles of neural computation. Recent advances in GEVIs have substantially improved their signal-to-noise ratio (SNR), enabling recordings from dozens of cells in superficial tissue using one-photon imaging[1–3]. There have also been improvements in instrumentation[4,5] and reporters[6] for 2P voltage imaging, enabling voltage imaging at depths up to 500 μm, though the number of simultaneously recorded cells at this depth remains < 3. Most applications of voltage imaging *in vivo* have been with 1P excitation [7–10], whereas for Ca^{2+} imaging, 2P microscopy is the dominant approach.[11] This raises the question: what are the scaling properties and relative merits of 1P vs 2P voltage imaging *in vivo*? How can a researcher considering a voltage imaging experiment decide which approach to use?

The physical requirements of Ca^{2+} imaging and voltage imaging differ substantially, so intuitions may not transfer. For Ca^{2+} imaging, typical events last 100 – 500 ms and have amplitudes of $\Delta F/F$ ~1. Signals come from the bulk cytoplasm. For voltage imaging, action potentials last ~0.3 – 2 ms, and typically have amplitudes of $\Delta F/F$ ~ 10%, though subthreshold events can be 100-fold smaller. Signals are localized to the cell membrane. Thus the key challenge in voltage imaging is to acquire adequate SNR in the presence of shot-noise and motion artifacts, while remaining at tissue-safe laser powers.

Shot noise imposes a fundamental limit on SNR. A source that generates, on average, N detected photons, will have fluctuations with standard deviation $\sqrt{N}$. To detect a 1 ms spike ($\Delta F/F$ ~ 10%) with an SNR of 10, requires determining fluorescence to 1% precision in 1 ms. We adopt 1% in 1 ms as a reasonable standard for a high-SNR voltage recording. Due to shot noise, this standard requires detecting at least 10^4 photons/ms, or 10^7 photons/s. For experiments solely focused on spike detection, a lower SNR may be acceptable. A minimal standard for spike detection in pyramidal cells is ~4% precision in 2.5 ms (i.e. 400 Hz recording). This minimal standard requires detecting 2.5×10^5 photons/s.

Filtering in space or time can increase the effective value of N at a given pixel, at the cost of lower spatial or temporal resolution, but filtering does not change the $\sqrt{N}$ shot noise scaling. Post-

processing, whether by linear filters or by nonlinear AI-based algorithms,[12] cannot overcome these fundamental limits. A detailed analysis of shot-noise constraints on spike detection has been published,[13] and these considerations have been applied in design of optimized 2P Ca^{2+} imaging protocols.[14]

We compared the brightness of commonly used voltage indicators in HEK293T (HEK) cells under alternating wide-field 1P illumination and 2P spiral illumination, using a shared detection path for both modalities to ensure equal photon detection efficiencies (Fig. 1a-c; Methods). We compared: a voltage sensitive dye (BeRST1[15]), opsin-based GEVIs (QuasAr6a[16] and Voltron2[17]), and GEVIs that couple a voltage sensitive phosphatase (VSP) to a circularly permuted partner fluorophore (ASAP3[4] and JEDI-2P[6]).

As expected, the fluorescence scaled linearly with 1P illumination intensity and quadratically with 2P intensity (Fig. 1d). For all but one indicator, 2P illumination required at least 10^4-fold greater time-averaged power per cell to achieve comparable counts to 1P illumination (Fig. 1e). The ratio of 2P to 1P powers for QuasAr6a was only ~300, due to the requirement for high-intensity 1P illumination. Consistent with prior reports,[1] we found that chemigenetic indicators were brighter than their purely protein-based counterparts, though our measurements did not assign the relative contributions of expression level vs. per-molecule brightness.

The huge difference in optical power requirement between 1P and 2P excitation is consistent with published reports: 2P imaging of JEDI-2P was reported at a power of 9 – 12 mW/cell[6], whereas 1P imaging of similar GFP-based GEVIs is typically performed at 1 – 10 W/cm^2,[4,6] corresponding to 1 – 10 μW/cell. Estimates based on tabulated 1P and 2P absorption coefficients[18] give a similar factor of ~10^4 difference in power efficiency (Supplementary text).

We then measured voltage sensitivity of one representative from each GEVI family, comparing 1P and 2P illumination. Using whole-cell voltage clamp in HEK cells (Fig. 1f), we found that the contrast (ΔF/F per 100 mV) of the VSP-based JEDI-2P was similar for 1P and 2P illumination. The opsin-based chemigenetic indicator Voltron2$_{525}$ showed voltage sensitivity under 1P but not 2P illumination (Fig. 1g-h). Loss of voltage sensitivity under 2P illumination of FRET-Opsin GEVIs has been reported previously[19], but the mechanism is unknown.

Shot noise places an upper bound on the number of cells which can be measured simultaneously via 2P illumination, N_{cells}^{2P}, with a given SNR. Under a protocol which sequentially visits single cells, N_{cells}^{2P} depends on both the brightness and voltage sensitivity (see Supplementary Information for derivation):

$$N_{cells}^{2P} = \frac{A \cdot \tau \cdot P^2 \cdot \beta^2 \phi}{SNR^2} \qquad [1]$$

Here A is the brightness coefficient derived from the HEK cell experiments (Eq. S1), τ is the integration time, P is the laser power at the focus, β is the fractional fluorescence contrast from a spike (ΔF/F per spike), ϕ is the fraction of the scan that intersects with the cell membrane, and SNR is the target SNR, defined as the ratio of the spike amplitude to shot noise. For an analysis that includes the effect of light scattering on depth-dependent collection efficiency, see [20].

The parameter ϕ approaches 1 for perfectly membrane-targeted illumination. To estimate ϕ for a raster scan over a bounding box around a single cell body, we examined 2P images of pyramidal cells with membrane-targeted fluorescent tags in cortex layer 2/3. In these images, the

membrane-labeled area fraction within the bounding box was ϕ_{bb} = 0.18 ± 0.07 (mean ± std, n = 10 cells). For a raster scan over multiple sparsely expressing cells, ϕ is lower than ϕ_{bb} by a factor of the sparsity. The low values of ϕ for raster-scanned 2P imaging are a consequence of the membrane-localized signal and highlight the importance of membrane-targeted illumination. However, precise targeting of the illumination to the membrane increases sensitivity to motion artifacts.

Eq. 1 can be used to predict the scaling of N_{cells}^{2P} as a function of depth, d, for 2P imaging of a GEVI. The power at a laser focus decays exponentially with d, with an extinction length in brain tissue at λ = 920 nm of l_e between 112[20,21] and 155 μm.[22] Substituting $P = P_0 e^{-d/l_e}$ into Eq. 1 implies a decay in N_{cells}^{2P} by a factor of 10 for every 130 - 180 μm increase in d (Supplementary Figure 1), assuming constant power P_0 into the tissue. To avoid tissue damage, the total power into the brain should be P_o < 200 mW in a typical 1 mm field of view.[23]

To test our predictions, we expressed soma-localized JEDI-2P in mouse cortex and performed structured illumination 1P imaging and raster-scanned 2P imaging at several depths (Fig. 2a-b; Methods). With 1P illumination, JEDI-2P-expressing cells were resolvable down to d ~ 200 μm. The challenge for 1P imaging at greater depths was not shot noise, but rather decrease in signal-to-background ratio. At depths > 200 μm, cells were not distinguishable from background by 1P imaging with 488 nm excitation (Fig. 2c).

With 2P illumination, cells were resolvable to d = 473 μm, the greatest depth we tested (Fig. 2b). As the cell depth increased, we increased the 2P laser power to maintain sufficient count rate to resolve the cells, up to P_0 = 140 mW at d = 473 μm. We applied Eq. 1 to the instantaneous count rates measured from the cell membranes (Fig. 2d) to estimate N_{cells}^{2P} for ϕ ~ 1, i.e., a perfectly membrane-targeted annular scan pattern. We assumed β = 0.1, a target shot noise-limited SNR of 10 in a 1 kHz bandwidth and extrapolated the count rates to an input power of P_0 = 200 mW. The predicted number of measurable cells decreased quickly at d > 200 μm and dropped below one at d > 470 μm and input power 200 mW (Fig. 2e). These results are similar to the prediction from a simple model using the 2P count rates from our HEK cell experiments (Supplementary Fig. 1a).

Eq. 1 places severe constraints on the number of cells that will be measurable at d > 200 μm with 2P voltage imaging, even with substantial improvements in GEVI brightness and voltage sensitivity (Supplementary Figure. 1b). These findings indicate that 2P imaging of hundreds of neurons with high SNR at depth > 200 μm will require orders-of-magnitude improvements in 2P GEVIs or qualitatively new approaches to imaging. The Supplemental Text analyzes the impact of laser repetition rate, optical focus shape (e.g. numerical aperture, Supplementary Fig. 2), and scan pattern. The most promising optical arrangement comprises excitation with high numerical aperture, low repetition rate (1 – 10 MHz), short pulses (< 100 fs), and membrane-targeted illumination with real-time compensation for tissue motion.

Acknowledgements. We thank Andrew Preecha and Shahinoor Begum for technical assistance, and Simon Kheifets and Vicente Parot for helpful discussions. This work was supported by NIH grant R01-NS126043.

Methods

HEK cell culture
HEK293T cells were maintained at 37 °C, 5% CO2 in Dulbecco's Modified Eagle Medium (DMEM) supplemented with 10% fetal bovine serum, 1% GlutaMax-I, penicillin (100 U/mL), streptomycin (100 mg/mL). For maintaining or expanding the cell culture, we used 35 mm TC-treated culture dish (Corning). For each imaging experiment, cells in one 35 mm dish were transiently transfected with the construct to be imaged using PEI in a 3:1 PEI:DNA mass ratio. For all the imaging experiments, cells were replated on glass-bottomed dishes (Cellvis, Cat.# D35-14-1.5-N) 36 hours after transfection. Imaging was performed ~6 hours after replating. Before optical stimulation and imaging, the medium was replaced with extracellular (XC) buffer containing 125 mM NaCl, 2.5 mM KCl, 3 mM CaCl2, 1 mM MgCl2, 15 mM HEPES, 30 mM glucose (pH 7.3). For BeRST1 experiments in HEK cells, cells were stained with 1 μM BeRST1 for 30 min prior to 3x wash with XC buffer before imaging.

Microscope and illumination control
All imaging was performed on a custom-built upright microscope equipped with 1P and 2P illumination paths and a shared emission path to an sCMOS camera (Hamamatsu, ORCA-Flash 4.0). The 1P illumination path contained a 488 nm laser (Coherent OBIS), a 532 nm laser (Laserglow LLS-0532) and a 635 nm laser (Coherent OBIS). The outputs of the 488 nm and 532 nm lasers were modulated using a multichannel acousto-optic tunable filter (Gooch & Housego PCAOM NI VIS driven by G&H MSD040-150). The 635 nm laser was modulated using its analog modulation input and an external neutral density filter wheel (Thorlabs). The 488 nm and 532 nm lasers were patterned via a Digital Micromirror Display (Vialux V-7001 V-module). To convert illumination intensity to power per cell, we approximated HEK cells as circles with a 10 μm diameter, e.g. an intensity of 1 W/cm^2 corresponded to 0.8 μW per cell.

The two-photon illumination path comprised an 80 MHz tunable femtosecond laser (InSight DeepSee, Spectra Physics), an electro-optic modulator (ConOptics 350-80-02) and two galvo mirrors for steering (Cambridge Technology 6215H driven by 6671HP driver). Power calibration was performed with a Thorlabs PM400 power meter with a photodiode-based sensor (S170C) and a thermal sensor (S175C) for 1P and 2P illumination, respectively. Electrical stimuli and measurements were performed using a National Instruments 6063 PCIe DAQ. All imaging was performed with a 25x water immersion objective (Olympus XLPLN25XWMP2, 2mm working distance, NA 1.05).

The excitation wavelengths used for 1P (2P) excitation of each of the GEVIs were: ASAP3 488 nm (930 nm), BeRST1 635 nm (850 nm), JEDI-2P 488 nm (930 nm), QuasAr6a 635 nm (900 nm), Voltron2$_{JF525}$ 488 nm (930 nm), Voltron2$_{JF585}$ 594 nm (1100 nm), Voltron2$_{JF669}$ 635 nm (1220 nm). At each wavelength the dispersion was adjusted to maximize the 2P fluorescence signal. The wavelengths for 2P excitation of QuasAr6a and BeRST1 were chosen to drive the S_0 to S_2 transition rather than the S_0 to S_1 transition because the S_2 transition was stronger.

Measuring voltage-sensitive fluorescence in vitro
All imaging and electrophysiology experiments were performed in XC buffer. Concurrent whole-cell patch clamp and fluorescence recordings were acquired on the microscope described above. Filamented glass micropipettes were pulled to a tip resistance of 5–8 MΩ and filled with internal solution containing 125 mM potassium gluconate, 8 mM NaCl, 0.6 mM $MgCl_2$, 0.1 mM $CaCl_2$, 1 mM EGTA, 10 mM HEPES, 4 mM Mg-ATP and 0.4 mM Na-GTP (pH 7.3), adjusted to 295 mOsm with sucrose. Whole-cell patch clamp recordings were performed with an Axopatch 200B amplifier (Molecular Devices). Fluorescence was recorded in response to a square wave from -70 mV to +30 mV.

In-house AAV packaging

AAV2/9 JEDI-2P vectors were packaged in house based on a published protocol[24]. Briefly, 50~70% confluent HEK293T cells grown in DMEM supplemented with 5% FBS were triple transfected with pHelper, pAAV ITRexpression, and pAAV Rep-Cap plasmids using acidified (pH 4) PEI (DNA:PEI ratio 1:3) in 1~2 T175 flasks (~2 x 10^7 cells/flask). The AAV-containing medium was harvested on Day 3, and the AAV-containing medium and cells were harvested on Day 5. For the second harvest, AAVs were released from the cells with citrate buffer (55 mM citric acid, 55 mM sodium citrate, 800 mM NaCl, 3 mL per flask). The two harvests were then combined and precipitated with PEG/NaCl (5x, 40% PEG 8000 (w/v), 2.5 M NaCl, 4 °C overnight). The low-titer virus was then purified with chloroform extraction (viral suspension and chloroform 1:1 (v/v)), aqueous two-phase partitioning (per 1 g of the AAV-containing supernatant, add 5 g of 20% $(NH_4)_2SO_4$ solution and 1.5 g of 50% PEG 8000 solution, and iodixanol discontinuous gradient centrifugation (15%, 25%, 40%, and 54% iodixanol gradient prepared from OptiPrep (60% (w/v) Iodixanol, Axis-Shield PoC AS). The purified AAV titer was determined via qPCR (SYBR Green, primer for forward ITR: 5'-GGAACCCCTAGTGATGGAGTT-3'; primer for reverse ITR sequence 5'- CGGCCTCAGTGAGCGA-3').

In vivo imaging

The cranial window surgery for *in vivo* imaging was based on previously published protocols[7]. Briefly, a CD1 mouse was injected with 50 nL viral mix in 4 sites in the whisker barrel cortex at 100, 200, 300, 400, and 500 μm below the tissue surface. Viral mix had a final concentration of 5e12 vg/mL pAAV-EF1a-DIO-JEDI-2P-Kv2.1motif and 1e11 CamKII-Cre in AAV 2/9. A cranial window and mounting plate were then installed over the injection sites. Two weeks after surgery and injection, a head fixed CD1 mouse was imaged at 1.5% isoflurane with the dose adjusted to maintain a stable breathing rate. Mouse was kept on a heating pad (WPI ATC2000) to maintain stable body temperature at 37 °C and its eyes were kept moist using ophthalmic eye ointment. 2P imaging was performed at a wavelength of 930 nm. Mouse was imaged for 2 hours after which it recovered in less than 10 minutes.

Light for 1P imaging *in vivo* was patterned off of a digital micromirror device to selectively illuminate the targeted cell body, as described above.

Figures

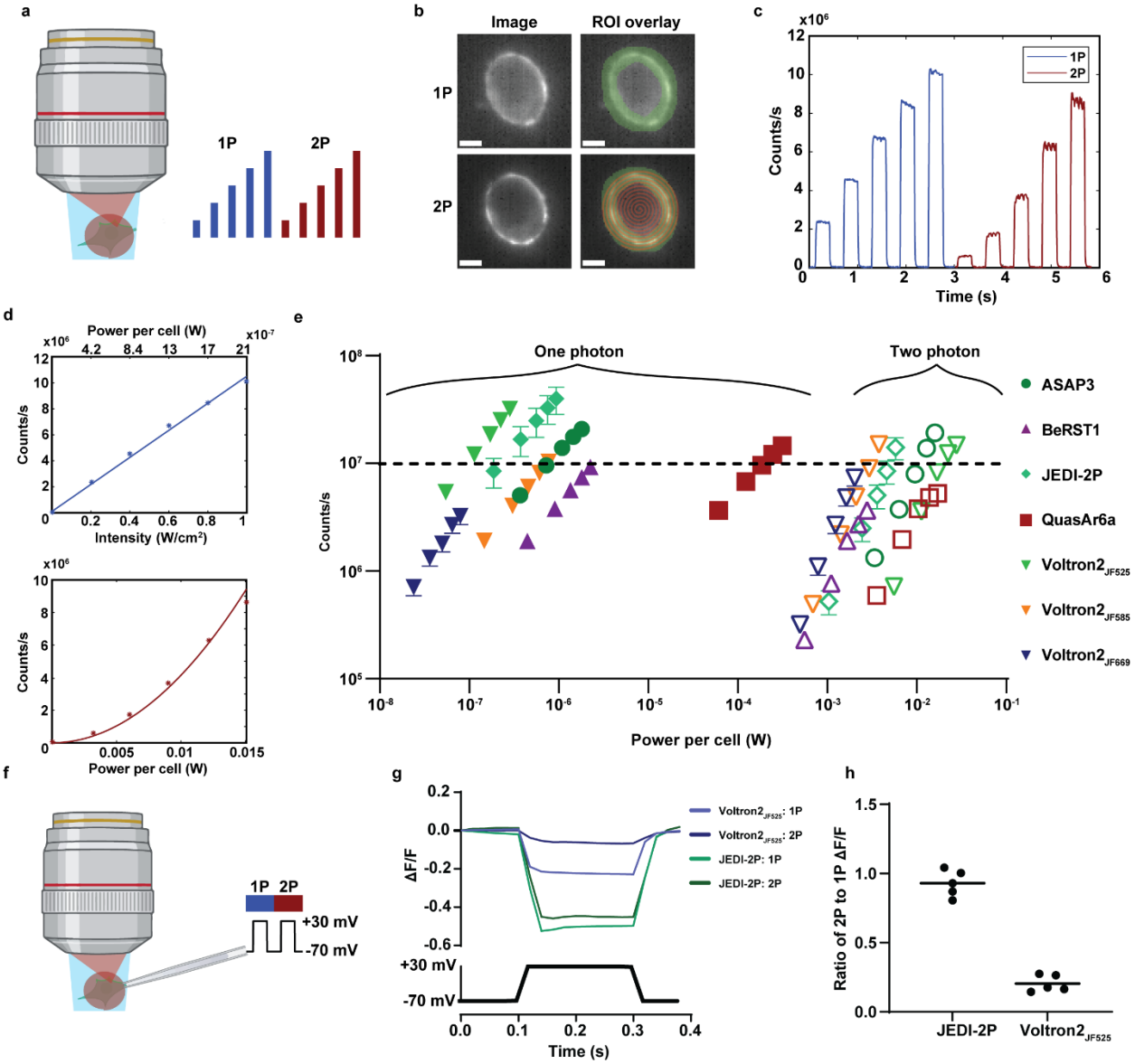

Figure 1. Comparison of 1P and 2P brightness and sensitivity of fluorescent voltage indicators. A) Diagram of experiment. HEK cells were sequentially illuminated with wide-field 1P light in steps of increasing intensity, then by spiral scan 2P steps of increasing intensity. B) Example HEK cell expressing the GEVI ASAP3. 2P spiral scan pattern shown in red and analysis ROI shown in green. Scale bars 5 μm. C) Example single-trial data for cell expressing ASAP3. D) Top: fluorescence in c as a function of 1P intensity with linear fit. Bottom: fluorescence as a function of 2P intensity with quadratic fit. E) Log-log plot of count rate vs. optical power on the cell for seven voltage indicators. 1P data: filled symbols, 2P data: empty symbols. Error bars are SEM from at least $n = 8$ cells. F) Whole-cell patch clamp protocol for measuring voltage sensitivity under 1P and 2P excitation. G) Average voltage responses of JEDI-2P and Voltron2$_{525}$ under 1P and 2P illumination. H) Ratio of voltage contrast under 2P vs. 1P illumination for JEDI-2P and Voltron2$_{525}$.

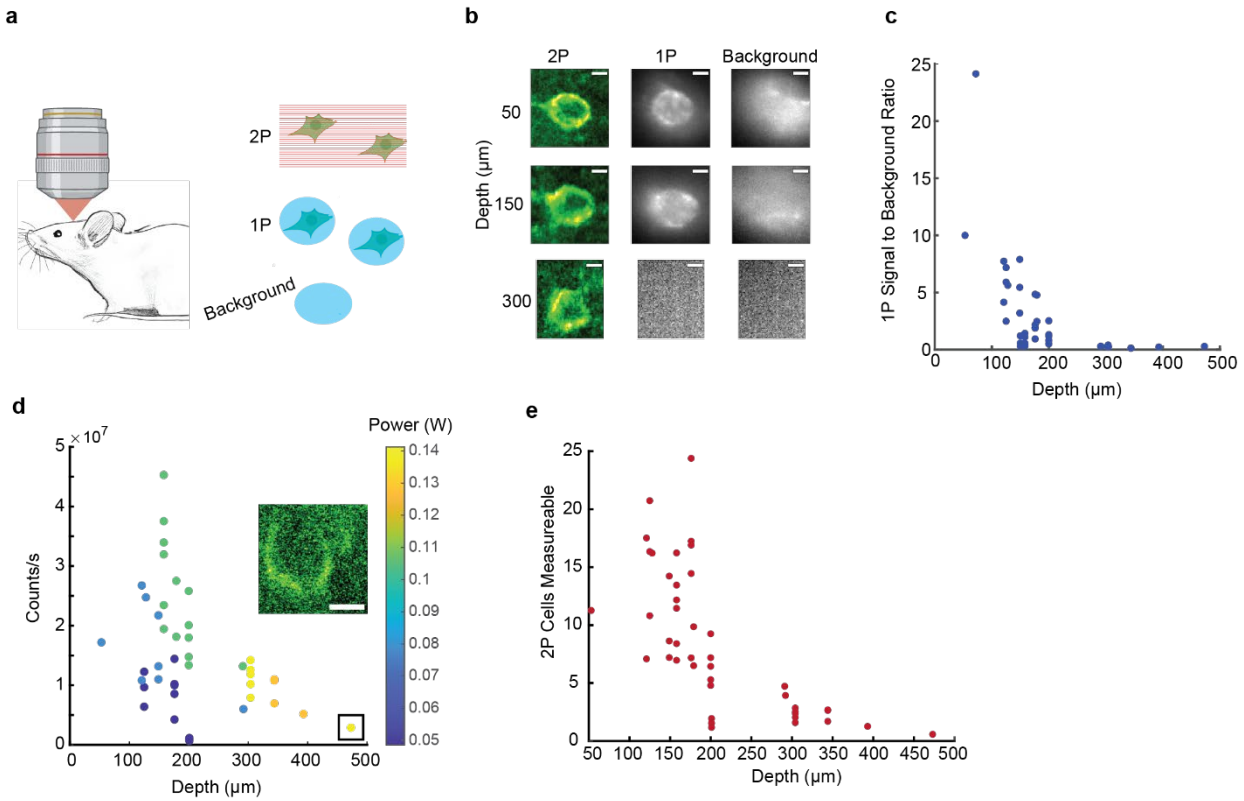

Figure 2. Depth-dependent 2P signal in brain. a) Experimental protocol. In a mouse expressing JEDI-2P, raster-scanned 2P (λ = 920 nm) and DMD-patterned 1P imaging (λ = 488 nm) were alternately applied to neurons at different depths. 1P illumination patterned to cell-free regions was used to estimate background signal. b) Example 1P and 2P images of cells at three depths. Scale bars 5 μm. c) Estimated signal-to-background ratio for neurons under patterned 1P illumination. d) Mean count rate from the membranes of 43 cells under 2P illumination. Color indicates excitation power. Inset shows cell at 473 microns of depth. (Scale bar 5 μm). e) Predicted number of simultaneously measurable cells at SNR=10 and 200 mW power for each single-cell count-rate reported in (d).

Supporting Information

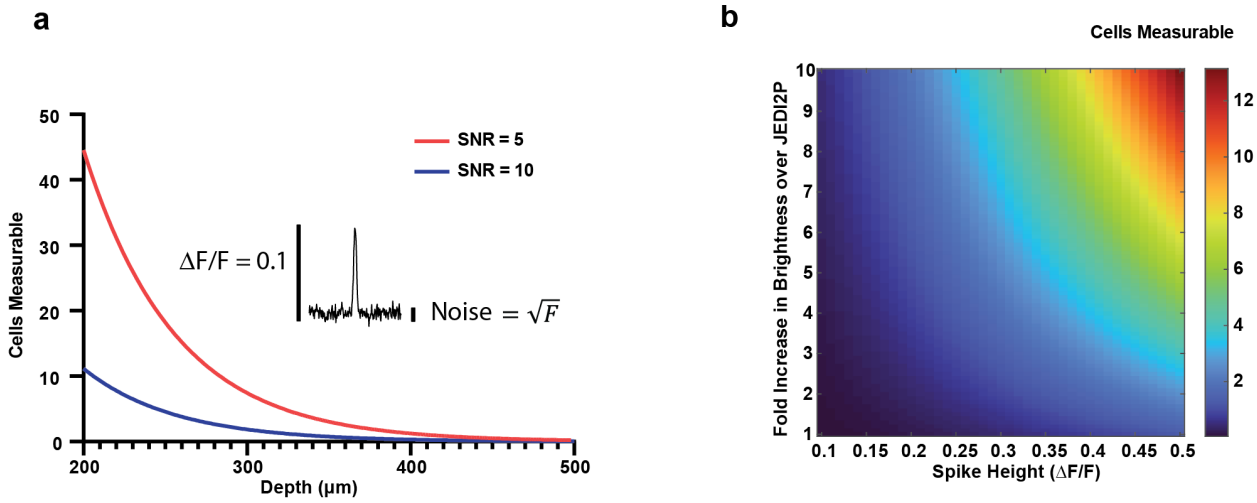

Supplementary Figure 1. Scaling of 2P voltage measurements with depth and with GEVI properties. a) Predicted number of simultaneously measurable cells as a function of depth, based on brightness derived from HEK cells expressing JEDI-2P (Fig. 1). We assumed a spike contrast of β = 0.1, target SNR of 5 or 10 in an integration time τ = 1 ms, a total power P_o = 200 mW, targeting fraction ϕ = 1, scattering length l_e = 112 μm[21]. b) Number of simultaneously measurable cells under 2P illumination at a depth of 500 μm, assuming brightness and contrast improvements of future GEVIs, and all other parameters as in (a).

Scaling of N_{cells}^{2P} with brightness and voltage sensitivity

Here we derive the dependence of the number of measurable cells on illumination intensity, fluorophore brightness, spike $\Delta F/F$, measurement bandwidth, and target SNR (Eq. 1 in the main text). We assume a point-scanning 2P illumination system which has perfect targeting to cell membranes and which can jump between cells with zero delay. This is a best-case scenario: motion artifacts, imperfect targeting, and scanner inertia or finite slew rates further degrade the SNR.

Let F (counts/s) be the detected fluorescence count rate from a single cell, let P (W) be the laser power at the focus. We define the constant for GEVI brightness, A, empirically as the proportionality between squared laser power and fluorescence signal.

$$F = A \cdot P^2, \qquad [S1]$$

where we have assumed that P is changed by adjusting total laser power, keeping laser repetition rate, pulse width, and focal and scan parameters constant.

Theoretically, A is given by:

$$A = \frac{\sigma^{2P} \times QY \times PDE \times N_{mol}}{Area^2} \qquad [S1.5]$$

where σ^{2P} is the 2P cross section, QY is the fluorescence quantum yield, PDE is the instrument photon detection efficiency, N_{mol} is the mean number of fluorophores in the 2P excitation volume

(see Fig. S2), and $Area$ is the cross-sectional area of the laser focus. We will not need this theoretical relation further.

The number of photons collected during a spike of duration τ is:

$$N_{photons} = A \cdot P^2 \cdot \tau \cdot \phi, \qquad [S2]$$

where ϕ is the fraction of the time that the laser focus intersects the cell membrane. Let β be the fractional change in fluorescence (ΔF/F) during a spike. If there is a contribution to the fluorescence from voltage-insensitive background, then β may be smaller than in the background-free case. The signal is:

$$S = \beta \cdot N_{photons} = \beta \cdot A \cdot P^2 \cdot \tau \cdot \phi \qquad [S3]$$

Assuming that the voltage change does not substantially affect the shot noise (i.e. $|\beta| \ll 1$), then the shot noise is:

$$Noise = \sqrt{N_{photons}} = \sqrt{A \cdot P^2 \cdot \tau \cdot \phi}. \qquad [S4]$$

Thus,

$$SNR = \frac{\beta \cdot N_{photons}}{\sqrt{N_{photons}}} = \beta \cdot P \cdot \sqrt{A \cdot \tau \cdot \phi}. \qquad [S5]$$

This SNR calculation is applicable only when the laser is targeted to a single cell. If the laser sequentially visits N cells, then the duty cycle on each cell is $1/N$. Assuming zero transit time between cells, the number of photons collected per cell scales inversely with the number of cells:

$$N_{photons} = \frac{A \cdot P^2 \cdot \tau \cdot \phi}{N_{cells}^{2P}}. \qquad [S6]$$

Therefore,

$$SNR = \beta \cdot P \cdot \sqrt{\frac{A \cdot \tau \cdot \phi}{N_{cells}^{2P}}}, \qquad [S7]$$

and

$$N_{cells}^{2P} = \frac{A \cdot \tau \cdot P^2 \cdot \beta^2 \cdot \phi}{SNR^2}. \qquad [S8]$$

Equation S8 shows the strong dependence of the number of measurable cells on the voltage sensitivity, β.

Scaling of N_{cells}^{2P} with GEVI kinetics

Some GEVIs have response times that are slow compared to the duration of a spike. On one hand, this blunts the amplitude of the spike response; on the other, it permits one to average for longer to detect whether a spike has occurred (assuming that the interval between spikes remains long compared to the response time of the GEVI). Here we analyze this tradeoff.

Consider a GEVI subjected to a voltage step which induces a steady-state change in fluorescence, $\frac{\Delta F}{F} = M$. Assume that the GEVI responds to a voltage step with an exponential response time

constant τ. Now consider the same GEVI subject to a voltage pulse of the same magnitude as before, and of duration $t_1 << \tau$. The amplitude of the GEVI response is $\beta = M\, t_1/\tau$. The signal can be integrated for time τ. Eq. S7 shows that $SNR \sim \tau^{-1/2}$. That is, faster GEVIs are better than slower ones in terms of shot noise-limited SNR, all else being equal.

Effect of optical parameters on 2P fluorescence

Our analysis above focused on the properties of the indicator. One can also analyze how changes to the illumination affect N_{cells}^{2P}.

Dividing the beam into multiple foci

We previously assumed that the laser was scanned sequentially among N cells. If the laser were split into N spots, each targeted to a different cell, while keeping total power constant, then the signal per spot would scale as $1/N^2$, while the duty cycle would increase from $1/N$ to 1. Thus the mean count-rate per cell would scale as $1/N$. Thus, splitting up the laser beam is generally not advantageous in terms of the tradeoff between signal and total laser power into the tissue.

However, if the illumination is limited by saturation of the 2P transition (see below) as opposed to total power into the sample, then there can be an advantage to splitting the laser into multiple foci while increasing total power up to the safe limit, to keep each focus near the 2P saturation limit.

Decreasing repetition rate

If the laser repetition rate is decreased by a factor of N while keeping total power constant, then signal per laser shot scales as N^2 (assuming no saturation of the excited state, see below), while the number of shots per second decreases by a factor of N, so the average signal increases by a factor of N. Lasers used for 2P imaging typically have a repetition rate of 80 MHz. This estimate suggests that lower repetition-rate lasers may be advantageous, though the repetition rate must be high enough to visit each cell at least once per measurement cycle. For example, an 800 kHz laser could visit 800 cells at a 1 kHz revisit rate (assuming a suitable scanner existed), and would provide 100-fold higher time-average count-rate (and 10-fold higher shot noise-limited SNR) than the same laser power delivered at 80 MHz.

Saturation of the 2P excitation typically occurs at pulse energies of ~1 nJ[25]. Furthermore, the peak intensity at the laser focus must not become too high or the sample may experience nonlinear photodamage.[26,27] Simultaneously approaching the 2P saturation energy (~1 nJ) and the maximum power into the sample (~200 mW) implies a depth-dependent optimum laser repetition rate of 1 – 10 MHz at depths of 5 l_a, where l_a is the exponential attenuation length.[25] Indeed a 2.5 MHz fiber-based soliton laser source was demonstrated to have 26-fold greater average signal than a matched 80 MHz Ti:S laser.[25]

Changing numerical aperture

The effect of numerical aperture (NA) on the 2P signal depends on the sample geometry. Within the Gaussian beam approximation, the width of the focus scales as

$$w_0 \sim \frac{1}{NA}.$$

The intensity, I, at the focus scales inversely with the cross-sectional area (so $I \sim NA^2$), and the rate of 2P excitation per molecule, Γ, scales with the intensity squared. Hence

$$\Gamma \sim NA^4.$$

The axial extent of the beam waist scales as

$$b \sim \frac{1}{NA^2}.$$

The total signal from a volume element depends on the number of fluorophores excited. In a three-dimensional bulk solution, the volume scales approximately as $V \sim w_0^2\, b \sim \frac{1}{NA^4}$. The total fluorescence signal F scales as $V \times \Gamma$. Hence, in bulk solution, $F \sim NA^0$. Fig. S2 shows the scaling for other geometries.

For 2P Ca^{2+} imaging, the signal is independent of NA provided that the beam waist remains within a single cell. In contrast, for 2P voltage imaging, the signal scales with NA with a dependence between linear and cubic, depending on whether the illumination is targeting a surface near the poles or equator; or targeting a neurite oriented along or perpendicular to the optical axis. This scaling argues for maximizing the NA for 2P voltage imaging. On the other hand, a smaller excitation spot leads to (a) a higher the rate of photobleaching and (b) greater sensitivity to misalignment between the focus and the sample, e.g. from sample motion.

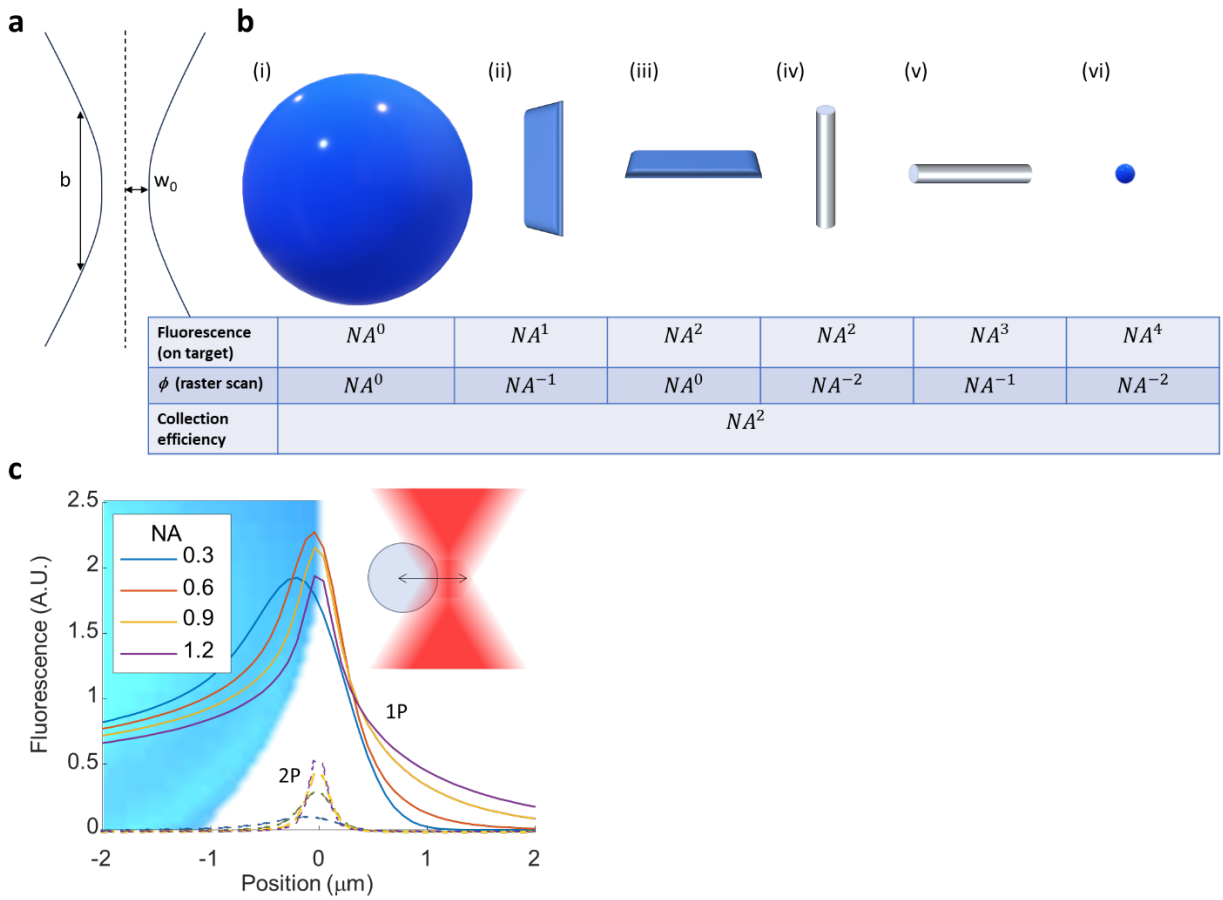

Fluorescence (on target)	NA^0	NA^1	NA^2	NA^2	NA^3	NA^4
ϕ (raster scan)	NA^0	NA^{-1}	NA^0	NA^{-2}	NA^{-1}	NA^{-2}
Collection efficiency	NA^2					

Figure S2. Scaling of fluorescence with numerical aperture, sample geometry, and excitation modality. (A) Geometry of a Gaussian beam, showing the width ($w_0 \sim 1/NA$) and waist ($b \sim 1/NA^2$). (B) Scaling of total 2P fluorescence as a function of excitation NA for different sample geometries. All slender dimensions are assumed to be << w_0 and all extended dimensions

are assumed to be >> b. In a planar raster scan, the fraction of time that a sub-wavelength structure is excited, ϕ, depends on the focus width and hence the NA. In cases (iii), (v), and (vi) we assume that the object is perfectly in focus, i.e. in the axial plane where focus size is minimum. The collection efficiency for all geometries depends on the collection solid angle ~ NA^2. To calculate total signal for targeted illumination, multiply the first and third lines; for a raster scan, multiply all three lines. Here we have assumed equal NA for excitation and collection, though this is not a requirement. (C) Total fluorescence evoked by the intersection of a laser focus and a spherical membrane, 10 μm diameter. We compared 1P and 2P excitation, with powers adjusted to match per-molecule excitation rates at the focus at NA 1.2. The much smaller 2P focal volume led to 5.3-fold smaller maximum fluorescence at the highest NA (and even greater discrepancy at lower NA) and 3-fold greater sensitivity to misalignment, compared to 1P excitation.

Optimizing the polarization

For membrane-localized chromophores, signal can be increased by aligning the excitation polarization with the transition dipole of the chromophore.[28] For 1P excitation, this effects scales as $\langle\theta^2\rangle$, where θ is the angle between the excitation polarization and the transition dipole, and the average is taken over all molecular orientations. For 2P excitation, this effect scales as $\langle\theta^4\rangle$, and can lead to several-fold polarization-dependent changes fluorescence signal from neurites with membrane-bound reporters.[29] Thus 2P voltage imaging systems could improve their power efficiency by selectively targeting cell membranes that have a favorable orientation relative to the laser polarization.

Theoretical comparison of 1P vs 2P photon efficiencies

We use the properties of JEDI-2P as an exemplary GEVI which works under both 1P and 2P excitation. We assume that the 1P and 2P absorption cross sections of the JEDI-2P chromophore are the same as for eGFP. While this assumption may not be exact, modest variations in these cross sections will not change the conclusion that 2P voltage imaging requires ~10^4-fold more power per cell.

First, we estimate the per-molecule excitation rate under 1P excitation. To achieve a per-cell detected photon count rate of 10^7 s^{-1}, required a mean per-cell laser power of 8×10^{-7} W, or equivalently an illumination intensity of ~1 W/cm² (Fig. 1; assuming a HEK cell is approximately 10 μm diameter). This intensity is in the middle of the range used for *in vivo* 1P voltage imaging: recordings of Voltron2 in flies used 200 – 1100 mW/cm²,[17] while high-speed recordings of PV cells in mice used up to 14 W/cm².[17]

The decadal molar absorption coefficient of eGFP is ε = 45,000 M^{-1} cm^{-1}.[30] The per-molecule excitation rate is:

$$\Gamma_{1P} = I\epsilon\frac{\lambda}{h\,c}\frac{10^3\ln 10}{N_A},$$

where I (W/cm²) is the incident intensity, ϵ (M^{-1} cm^{-1}) is the decadal molar absorption coefficient, λ (m) is the wavelength, h (6.63×10^{-34} J s) is Planck's constant, c (3×10^8 m/s) is the speed of light, and N_A (6.02×10^{23} mol^{-1}) is Avogadro's number. We assume λ = 488 nm and find that at I = 1 W/cm², $\Gamma_{1P} = 430\ s^{-1}$; at 10 W/cm², $\Gamma_{1P} = 4300\ s^{-1}$.

Assuming an overall 10% total light collection efficiency (reasonable for a high NA optical system), 10^7 detected photons/s corresponds to 10^8 emitted photons/s. At a per-molecule emission rate of 430 s^{-1}, this implies 2.3×10^5 molecules/cell. At a typical HEK cell membrane surface area of 1000 μm^2,[31] the density of reporters is 230 μm^{-2}.

We now estimate the 2P power needed to match the emitted count rate of 10^8 s^{-1}. The probability that a fluorophore is electronically excited by a single pulse from a 2P optical system is:[32]

$$P_{2P} = \frac{\sigma_2 P_{avg}^2}{\tau_{2P} f_{2P}^2}\left(\frac{[NA]^2}{2\hbar c\lambda}\right)^2,$$

where σ_2 is the 2P absorption cross section (m^4 s), P_{avg} (W) is the time-average power from the laser, τ_{2P} (s) is the pulse duration, f_{2P} is the laser repetition frequency, *NA* is the objective lens numerical aperture, and $\hbar$, c, and λ are as above. The per-molecule rate of excitation is $\Gamma_{2P} = f_{2P}P_{2P}$.

We assume parameters typical of a 2P imaging experiment: NA = 1, λ = 920 nm, τ_{2P} = 200 fs, f_{2P} = 80 MHz. The 2P absorption cross section of eGFP is σ_2 = 39 GM (39×10^{-58} m^4 s).[30]

The brightest signal from the cell arises when the laser focus intersects an equatorial membrane, so the optical axis lies in the plane of the membrane, as in Fig. S2c. In this case the membrane area that is optically excited is approximately $A_{2P} = w_0 b$, where w_0 is the waist of the Guassian focus and b is the depth of focus. The focus waist is approximately $w_0 = \frac{\lambda}{2NA}$, and the depth of focus is $b = 2\pi w_0^2 n/\lambda$, where n = 1.33 is the index of refraction. This estimate yields A_{2P} ~ 1 μm^2, implying that ~230 reporter molecules are in the 2P focus. To achieve a total emitted photon rate of 10^8 s^{-1} then implies a per-molecule emission rate of Γ_{2P} = 4.3×10^5 s^{-1}. The time-average laser power to achieve this count rate is 8 mW, 10^4-fold higher than the 1P power to achieve the same count rate. In the minimal SNR limit of 2.5×10^5 detected photons/s/cell (corresponding to 2.5×10^6 emitted photons/s/cell), the minimum time-average 2P power per cell is 0.4 mW (assuming ϕ = 1).

Citations

1. Abdelfattah, A. S. *et al.* Bright and photostable chemigenetic indicators for extended in vivo voltage imaging. *Science* **365**, 699–704 (2019).

2. Kannan, M. *et al.* Dual-polarity voltage imaging of the concurrent dynamics of multiple neuron types. *Science* **378**, eabm8797 (2022).

3. Weber, T. D., Moya, M. V., Kılıç, K., Mertz, J. & Economo, M. N. High-speed multiplane confocal microscopy for voltage imaging in densely labeled neuronal populations. *Nat Neurosci* **26**, 1642–1650 (2023).

4. Villette, V. *et al.* Ultrafast Two-Photon Imaging of a High-Gain Voltage Indicator in Awake Behaving Mice. *Cell* **179**, 1590-1608.e23 (2019).

5. Sims, R. R. *et al.* Scanless two-photon voltage imaging. *Res Sq* rs.3.rs-2412371 (2023) doi:10.21203/rs.3.rs-2412371/v1.

6. Liu, Z. *et al.* Sustained deep-tissue voltage recording using a fast indicator evolved for two-photon microscopy. *Cell* **185**, 3408-3425.e29 (2022).

7. Adam, Y. *et al.* Voltage imaging and optogenetics reveal behaviour-dependent changes in hippocampal dynamics. *Nature* **569**, 413–417 (2019).

8. Fan, L. Z. *et al.* All-optical physiology resolves a synaptic basis for behavioral timescale plasticity. *Cell* **186**, 543-559.e19 (2023).

9. Böhm, U. L. *et al.* Voltage imaging identifies spinal circuits that modulate locomotor adaptation in zebrafish. *Neuron* **110**, 1211-1222.e4 (2022).

10. Kim, T. H. & Schnitzer, M. J. Fluorescence imaging of large-scale neural ensemble dynamics. *Cell* **185**, 9–41 (2022).

11. Zong, W. *et al.* Large-scale two-photon calcium imaging in freely moving mice. *Cell* **185**, 1240-1256.e30 (2022).

12. Platisa, J. *et al.* High-speed low-light in vivo two-photon voltage imaging of large neuronal populations. *Nat Methods* **20**, 1095–1103 (2023).

13. Wilt, B. A., Fitzgerald, J. E. & Schnitzer, M. J. Photon Shot Noise Limits on Optical Detection of Neuronal Spikes and Estimation of Spike Timing. *Biophysical Journal* **104**, 51–62 (2013).

14. Friedrich, J. *et al.* Multi-scale approaches for high-speed imaging and analysis of large neural populations. *PLOS Computational Biology* **13**, e1005685 (2017).

15. Huang, Y.-L., Walker, A. S. & Miller, E. W. A Photostable Silicon Rhodamine Platform for Optical Voltage Sensing. *J. Am. Chem. Soc.* **137**, 10767–10776 (2015).

16. Tian, H. *et al.* Video-based pooled screening yields improved far-red genetically encoded voltage indicators. *Nat Methods* 1–13 (2023) doi:10.1038/s41592-022-01743-5.

17. Abdelfattah, A. S. *et al.* Sensitivity optimization of a rhodopsin-based fluorescent voltage indicator. *Neuron* **111**, 1547-1563.e9 (2023).

18. Xu, C. & Webb, W. W. Measurement of two-photon excitation cross sections of molecular fluorophores with data from 690 to 1050 nm. *J. Opt. Soc. Am. B, JOSAB* **13**, 481–491 (1996).

19. Brinks, D., Klein, A. J. & Cohen, A. E. Two-Photon Lifetime Imaging of Voltage Indicating Proteins as a Probe of Absolute Membrane Voltage. *Biophysical Journal* **109**, 914–921 (2015).

20. Oheim, M., Beaurepaire, E., Chaigneau, E., Mertz, J. & Charpak, S. Two-photon microscopy in brain tissue: parameters influencing the imaging depth. *J.Neurosci.Methods* **111**, 29–37 (2001).

21. Tran, A. P. & Jacques, S. L. Modeling voxel-based Monte Carlo light transport with curved and oblique boundary surfaces. *JBO* **25**, 025001 (2020).

22. Wang, M. *et al.* Comparing the effective attenuation lengths for long wavelength in vivo imaging of the mouse brain. *Biomed. Opt. Express, BOE* **9**, 3534–3543 (2018).

23. Podgorski, K. & Ranganathan, G. Brain heating induced by near-infrared lasers during multiphoton microscopy. *Journal of Neurophysiology* **116**, 1012–1023 (2016).

24. Kimura, T. *et al.* Production of adeno-associated virus vectors for in vitro and in vivo applications. *Sci Rep* **9**, 13601 (2019).

25. Charan, K., Li, B., Wang, M., Lin, C. P. & Xu, C. Fiber-based tunable repetition rate source for deep tissue two-photon fluorescence microscopy. *Biomed Opt Express* **9**, 2304–2311 (2018).

26. Donnert, G., Eggeling, C. & Hell, S. W. Major signal increase in fluorescence microscopy through dark-state relaxation. *Nature Methods* **4**, 81–86 (2007).

27. Ji, N., Magee, J. C. & Betzig, E. High-speed, low-photodamage nonlinear imaging using passive pulse splitters. *Nat Methods* **5**, 197–202 (2008).

28. Bloxham, B., Brinks, D., Kheifets, S. & Cohen, A. E. Linearly polarized excitation enhances signals from fluorescent voltage indicators. *Biophys J* **120**, 5333–5342 (2021).

29. Pulin, M. *et al.* Orthogonally-polarized excitation for improved two-photon and second-harmonic-generation microscopy, applied to neurotransmitter imaging with GPCR-based sensors. *Biomed. Opt. Express, BOE* **13**, 777–790 (2022).

30. Drobizhev, M., Makarov, N. S., Tillo, S. E., Hughes, T. E. & Rebane, A. Two-photon absorption properties of fluorescent proteins. *Nat Methods* **8**, 393–399 (2011).

31. Bandmann, V. *et al.* Membrane capacitance recordings resolve dynamics and complexity of receptor-mediated endocytosis in Wnt signalling. *Sci Rep* **9**, 12999 (2019).

32. Denk, W., Strickler, J. & Webb, W. Two-photon laser scanning fluorescence microscopy. *Science* **248**, 73–76 (1990).